Revista de Metalurgia
April-June 2023, 59 (2), e243
ISSN-L: 0034-8570
https://doi.org/10.3989/revmetalm.243

Effect of Ni on microstructure and wear behaviour of 13Cr-W-Mo-2C white cast iron

Tanju Teker[a], S. Osman Yılmaz[b]

[a] Sivas Cumhuriyet University, Faculty of Technology, Department of Manufacturing Engineering, 58140, Sivas, Türkiye

[b] Tekirdağ Namık Kemal University, Faculty of Engineering, Department of Mechanical Engineering, 59560, Çorlu, Tekirdağ, Türkiye

(*Corresponding author: tanjuteker@cumhuriyet.edu.tr)

Submitted: 8 December 2022 ; Accepted: 11 October 2023; Available On-line:

ABSTRACT: The effect of Ni concentration on the microstructure and wear performance of 13Cr-(0.5-7.0) Ni-W-Mo-Mn-2C white cast iron subjected to homogenization heat treatment was examined. Concentration of Ni was altered in the range 0.5-7.0 wt.% to obtain a stable microstructure against for dry sliding wear resistance as long sliding distance. The effect of Ni on the microstructure was analysed by X-ray diffraction, scanning electron microscopy, energy dispersive x-ray spectroscopy, elemental mapping and hardness. The wear performances were tested under the loads of 40, 90 and 140 N. Differential thermal analysis of samples with dissimilar Ni values was performed. The increase of Ni concentration decreased the secondary arm spacing of dendrites, refined the dendritic structure and raised the eutectic carbide ratio. The greatest wear performance was obtained for the sample having Ni over 6 wt.%.

KEYWORDS: Hardness; HCrWCI; Microstructure; Nickel; Wear

Citation/Citar como: Teker, T.; Yilmaz, S.O. (2023). "Effect of Ni on microstructure and wear behaviour of 13Cr-W-Mo-2C white cast iron". *Rev. Metal.* 59(2): e243. https://doi.org/10.3989/revmetalm.243

RESUMEN: *Efecto del Ni en la microestructura y el comportamiento frente al desgaste de la fundición blanca 13Cr-W-Mo-2C*. Se examinó el efecto de la concentración de Ni en la microestructura y el comportamiento frente al desgaste de la fundición blanca 13Cr-(0.5-7.0)Ni-W-Mo-Mn-2C sometida a tratamiento térmico de homogeneización. La concentración de Ni se modificó en el rango 0.5-7.0 % en peso para obtener una microestructura estable frente para la resistencia al desgaste por deslizamiento en seco para una larga distancia de deslizamiento. El efecto del Ni en la microestructura se analizó mediante difracción de rayos X, microscopía electrónica de barrido, espectrometría de energía dispersiva, mapeado químico elemental y dureza. Las prestaciones frente al desgaste se ensayaron con cargas de 40, 90 y 140 N. Se realizó un análisis térmico diferencial de las muestras con distintos valores de Ni. El aumento de la concentración de Ni redujo el espaciado entre los brazos secundarios de las dendritas, afinó la estructura dendrítica y aumentó la proporción de carburo eutéctico. El mayor rendimiento frente al desgaste se obtuvo en la muestra con Ni superior al 6 % en peso.

PALABRAS CLAVE: Dureza; HCrWCI; Microestructura; Níquel; Desgaste.

ORCID ID: Tanju Teker (https://orcid.org/0000-0001-7293-0723); S. Osman Yılmaz (https://orcid.org/0000-0001-7593-6135)

1. INTRODUCTION

HCrWCIs are sub-eutectic, eutectic or hypereutectic compounds. HCWCIs are employed as materials having 10-30 wt.% Cr and 2.0-3.5 wt.% C. The high nominal chromium content helps to prevent graphite formation and stabilize carbides. Also, copper, manganese, nickel and molybdenum are inserted to press the happen of pearlite during cooling. Materials with high chromium are used to make tools such as pumping, grinding and milling devices which are necessary for the processing of hard materials as cement, gravel, ore and coal (Powell and Bee, 1996; Tabrett and Sare, 2000; Zhang *et al*., 2001; Bedolla *et al.*, 2003; Wang *et al.*, 2006). The white cast iron microstructure is the same as the metal matrix composites. Austenite is a basic structure often encountered in cast high Cr metals. Moreover, the carbide in the structure of such alloys is M_7C_3 (M=Fe, Cr). This carbide grows like blades and rods parallel to the line of heat flow in the mould (Turenne *et al*., 1989; Powell and Laird II, 1992; Lu *et al*., 2006; Zhi *et al*., 2008). The microstructure and strength properties of high chromium white cast iron (HCrWCI) are influenced by the eutectic carbide ratio, the matrix microstructure and the secondary carbides embedded in the matrix (Tang *et al*., 2009; Scandian *et al*., 2009). The presence of secondary carbides advances the wear performance of the composite. The properties of secondary and eutectic carbides are remarkably altered by heat treatment, the ratio of major components (C, Cr) and alloying elements (Mo, W, V, Ti, Nb) (Mousavi Anijdan *et al*., 2007; Chung *et al*., 2009; Filipovic *et al*., 2013). These materials have excellent wear resistance, since there is eutectic or proeutectic M_7C_3 carbides in a more ductile matrix of alloys with high concentrations of Cr. The toughness of the matrix and the type of eutectic carbides or hard carbides (M_7C_3) provide high wear resistance (Aso *et al.*, 2001; Kasama *et al*., 2004). The significant microstructural parameters of wear resistance of high chromium content materials include the morphology, amount, orientation and interface of the carbides. The fracture toughness and hardness of the material are also influenced by these factors. The wear performance is specified as a function of heat treatment parameters and chemical composition. All alloy systems should be assessed in consideration of these factors and the tribological environment (Pearce, 1983; Hanlon *et al*., 1999; Wang *et al*., 2009; Mandal *et al*., 2017). Lin *et al*. (2010) investigated the effect of V, Mo, and Ni additions on the morphology and strength of carbides and eutectic clusters in Cr-Fe-C hard alloys with hypereutectic composition. Addition of V, Mo and Ni provided full performance in Cr–Fe–C hard-filled alloys. Chandan *et al*. (2022) reported the effect of Ni addition on the deformation and hardness of Fe40Mn40Co10Cr10 alloy during high pressure torsion machining. The Ni addition provided a four-fold increase in dislocation density and high hardness.

In this study, the effect of Ni concentration variation on the microstructure and wear performance of 13Cr-(0.5-7)Ni-W-Mo-Mn-2C white cast iron subjected to homogenization heat treatment was investigated.

2. MATERIALS AND METHODS

The chemical composition of the samples used for the study is given in Table 1. 13Cr-W-Mo-2C materials were melted in a medium frequency induction furnace of 10 kg. 0.5-7.0 wt.% Ni was added to the composition for austenite matrix stabilization. 75 wt.% FeSi was inserted to the crucible to minimize oxidation and slag. The melt was heated to 1560 °C and poured into CO_2-silicate molds at 1450 °C. The dimensions of the sample are 50×50×10 mm^3. The heat treatment of the samples is given in Table 2. Homogenization heating process utilized in this study contained annealing in argon atmosphere at 1000 ºC for a period of 6 h, followed by air-cooling.

The samples were polished and then etched in a solution of (5 g $FeCl_3$, 30 ml HCl, and 100 ml distilled water). Metallographic evaluation of samples was analyzed by X-ray diffraction (XRD: Bruker) and scanning electron microscopy (SEM: ZEISS EVO LS10), energy dispersive spectrometry (EDS), elemental mapping. A QNESS Q10M device was used to perform microhardness measurements with the HV scale under a 100 g load. Differential ther-

Table 1. The chemical composition of the 13Cr-Ni-W-Mo-Mn-2C

Chemical composition (wt.%)											
Elements	Fe	C	Mn	Si	Ni	Mo	Cr	W	S	P	Cu
(wt.%)	Bal.	2.3	0.5	1.6	0.5-7.0	3.2	13	1.2	0.03	0.03	0.20

Table 2. The heat treatment of the experimental samples

Sample	Composition	Heat treatment
S-Ref.	13Cr-W-Mo-Mn-2C	-
S1	13Cr-1Ni-W-Mo-Mn-2C	6 h, 1000 °C, air cooling
S2	13Cr-2Ni-W-Mo-Mn-2C	6 h, 1000 °C, air cooling
S3	13Cr-4Ni-W-Mo-Mn-2C	6 h, 1000 °C, air cooling
S4	13Cr-6Ni-W-Mo-Mn-2C	6 h, 1000 °C, air cooling
S5	13Cr-7Ni-W-Mo-Mn-2C	6 h, 1000 °C, air cooling

mal analysis of the samples was performed (DTA: SHIMADZU TG-DTA). Under the loads of 40, 90, and 140 N), wear tests were done on a pin-on-disc wear machine (model: UTS Tribometer T10/20) according to the ASTM-G65 Standard. All tests were performed with a wear test time of 60 s. The wear rates were obtained by measuring the sample masses before and after the wear tests. Worn surfaces were examined by SEM.

3. RESULTS

3.1. Microstructure and hardness

SEM micrograph of hypoeutectic as-cast 13Cr-W-Mo-Mn-2C white cast iron is shown in Fig. 1. Microstructure comprised a typical eutectic structure (matrix) and large hexagonal-shaped M_7C_3 carbides. The as-cast state had M_7C_3 carbides in the austenitic matrix. After a destabilization heat treatment, the matrix microstructure became heavily formation of secondary carbides within the austenite dendrite (Fig. 2).

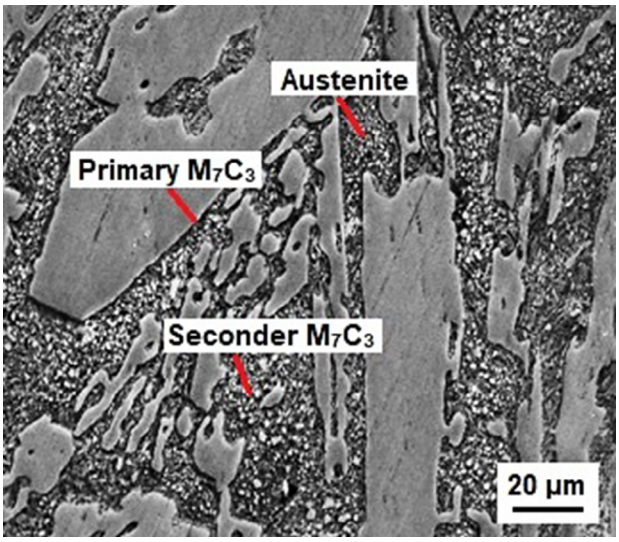

Figure 1. SEM micrographs of as-cast 13Cr-W-Mo-Mn-2C white cast iron.

The typical microstructures of samples having different Ni concentration of 1, 2, 4, 6, 7 wt.% and as-heat treated circumstances (6 h, 1000 °C, air cooling) are shown in Fig. 2a-e. After the heat treatment, the dendritic structure disrupted, the continuity of dendritic carbides was cut and the carbides started to shrink. A significant fraction of retained austenite still remained after heat treating between M_7C_3 carbides which is thought to be due to the alloys higher Ni content (>4). The presence of high Ni content around the austenite dendrite will tend to stabilize the remaining austenite where Ni is completely rejected by the carbide phase. The heat treatment time duration was effective especially on the derogation of the M_7C_3 carbides. The rejection of Ni to austenite phase softened the transformation of austenite to martensite, and suppressed the martensite start temperature. The most fundamental phases in white cast irons were austenite, martensite and pearlite. The hardness, toughness and abrasive characteristics of the structure depend on the ratio of these phases (Biner, 1985). The samples studied here were hypoeutectic white cast irons, and the first matrix phase was the austenite. This phase forming as the first nucleolus during solidification evolve to the form of dendrite arms with different shapes based on the thermal gradient. Austenite crystals had a certain carbon equivalent. This carbon equivalent is created by elements such as C, Mn, Ni and Mo. As the C concentration in the matrix structure increases, the lattice parameter in the body-centered cubic atomic crystal also increases. The carbon concentration in the austenite may change between 2.11% and 0.30% based on the concentration of Cr in the austenite. At room temperature, the solubility of the C equivalent in the austenite was approximately zero. C had the most effective role in the stability of the austenite phase in room temperature. C was the most important factor in reducing the martensite initiation temperature to lower values. If the transition to the pearlite phase is wanted to be prevented from the austenite phase with high-C content, then the structure is cooled down to room temperature, and the appearing phase remainder becomes austenite (Biner, 1985; Lin *et al.*, 2010; Chandan *et al.,* 2022).

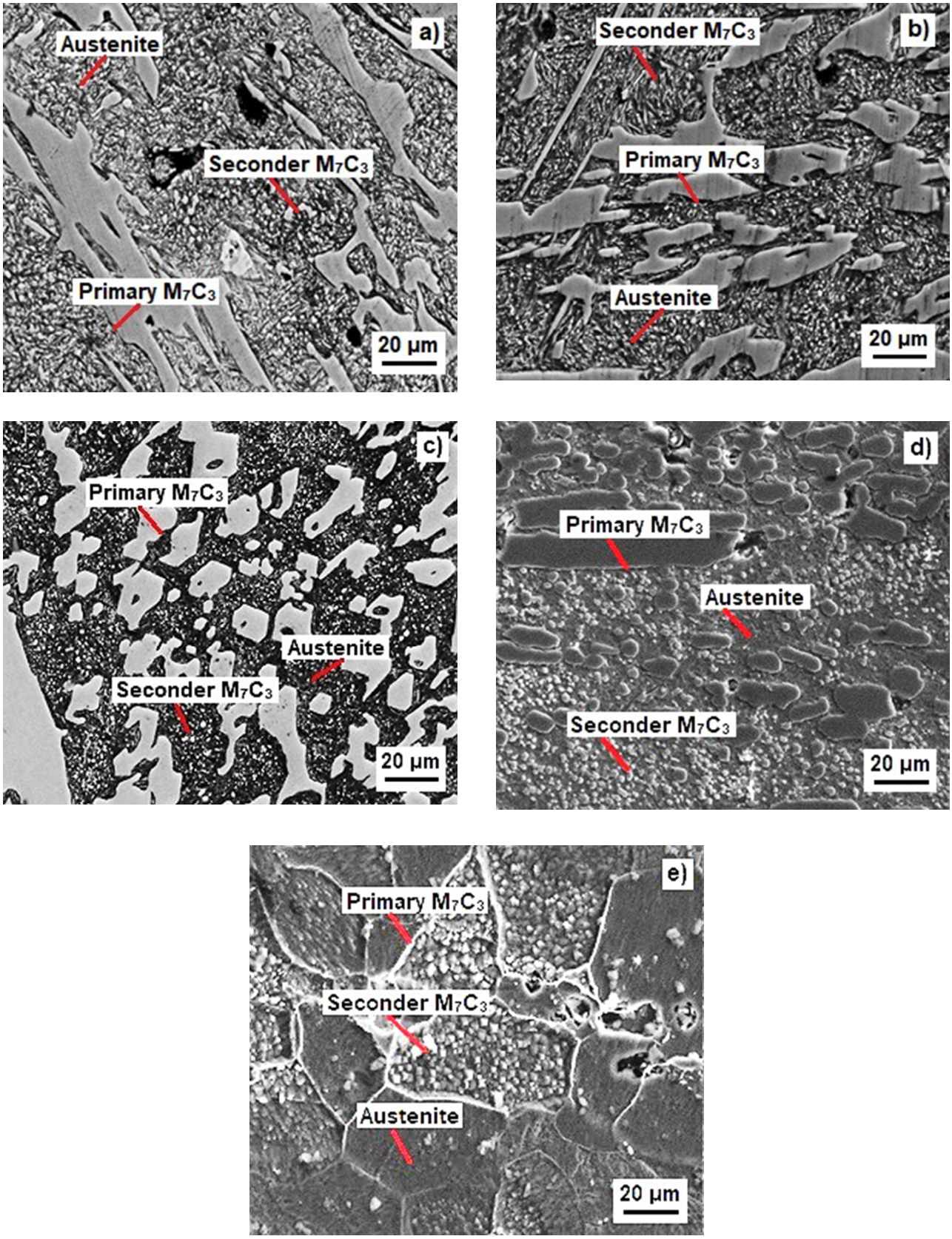

Figure 2. SEM micrographs of a) S1, b) S2, c) S3, d) S4, e) S5 samples.

SEM micrographs of the microstructure showing the changes created by Ni addition are shown in Fig. 2. The presence of Ni had a substantial impact on the arm spacing of the carbides. There were microstructural differences in the arm length of carbides and carbide vol.%. The additions of Ni were increased arm spacing of carbides, and the carbide volume fraction from 0.20 to 0.30 for 0.5-7.0 wt.%. The increase of the Ni concentration caused destabilisation of the M_3C phase, replaced by M_7C_3 eutectic carbide phase, and broke the dendritic morphology (Fig.2e) (Laird *et al.,* 2000). In addition, the presence of 2-7 wt.% Ni in the structure allows the virgin austenite to approach the Ms temperature unimpeded by the creation of pearlite. The microstructure of as-cast structure having 2-7 wt.% Ni included austenite-martensite phase mixture. Together with Ni, the concentration of Cr was important in the formation of carbide type of the structure during solidification (Laird *et al.,* 2000). The presence of Cr over 5 wt.% in this alloy having high Ni concentration formed the refined M_7C_3 carbides. Ni concentration above 6 wt.% produced a homogeneously dispersed microstructure with M_7C_3 carbides lower than 2 μm (Fig. 2e).

The heat-treated samples shown in Fig. 2 had a microstructure that differed significantly from the cast structure (Fig. 1). The biggest difference lies in transformation of austenite to martensite and the increase in M_3C secondary carbide concentration. The hardness results of experimental samples are given in Fig. 3. The increase of Ni had a great influence on hardness according to the as-cast condition. However, there were a little rise on the hardness for the additions of Ni over 2 wt.% in the heat-treated condition. Heat treatment eventuated in a significant hardness change. The matrix hardness was 400 HV in the as-cast sample, it was 781 HV in the 5 wt.% Ni sample. This rise was caused probably by solid solution treatment leading to dissolution of Si in the austenitic structure. Microhardness increased from 576 to 731 HV in the sample with 7 wt.% Ni. Fig. 3 also indicates that the hardness decreased adjacent to the surface due to fine, rod and blade type M_7C_3 carbides and small proeutectic austenite dendrites. Further away from the surface, the austenite dendrites became larger and carbide morphology became more blades like. The fine dendritic structure transformed to coarser structure as function of solidification rate. The increase in hardness presented an interesting relationship between the microstructures of the samples during heat treatment. This relation was not only depending on the concentration of martensite, the presence of tiny secondary carbides was primarily effective on the degree of hardness and toughness.

The XRD pattern of the steel with 7 wt.% Ni content (S5) is displayed in Fig. 4. The samples contained hard eutectic carbides embedded in an austenite matrix. The matrix consisted mainly of austenite dendrites. The austenite was surrounded by M_7C_3 carbides. This carbide was embedded in a martensitic matrix which contains retained austenite as an outcome of heat treatment in the microstructure. Austenite and martensite phases were supersaturated with carbon and other alloying elements. This led to a decrease in Ms (initial temperature of the martensitic transition) and the preservation of a high amount of austenite at room temperature for the samples having Ni over 6 wt.%.

Chemical composition clarified by EDS of the steel with 7 wt.% Ni content (S5) is shown in Fig. 5 and results verify the phases as M_7C_3. Figure 6 demonstrates the SEM mapped image analysis of the sample S5. Mn, Si, W, Mo, Ti, Ni, C, Cr and Fe elements are presented in the sample. Note that there was a hypoeutectic composition for 0.5 wt.% Ni within the austenite phase interval in the alloy. The 2 wt.% Ni alloy (S2) was near to the eutectic phase, while the alloys with 4-5 wt.% Ni content had a hypereutectic composition where solidification began with the formation of M_7C_3. The addition of up to 6 wt.% Ni (S4) increased the amount of austenite retained in the cast structure from about ~65 vol.% to ~70 vol.%. For samples containing 7 wt.% Ni (S5), the composition was stable at ~25% under

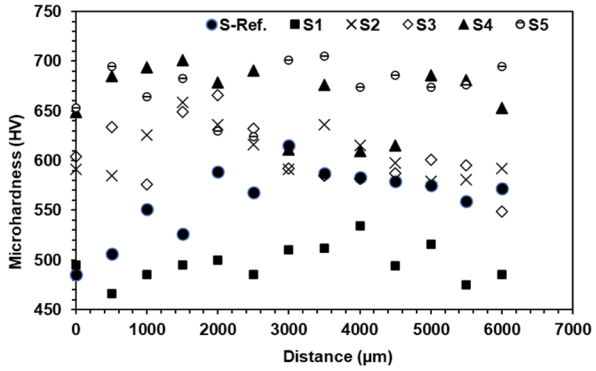

Figure 3. The hardness results for experimental samples.

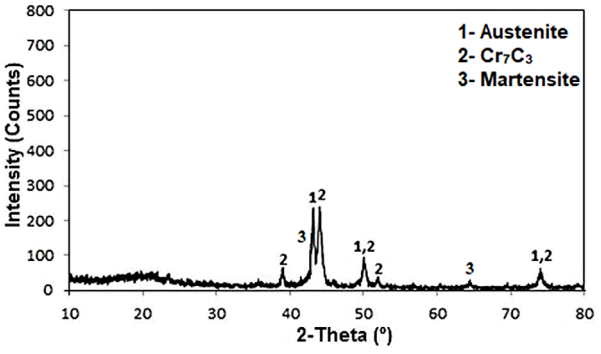

Figure 4. X-ray pattern of sample S5.

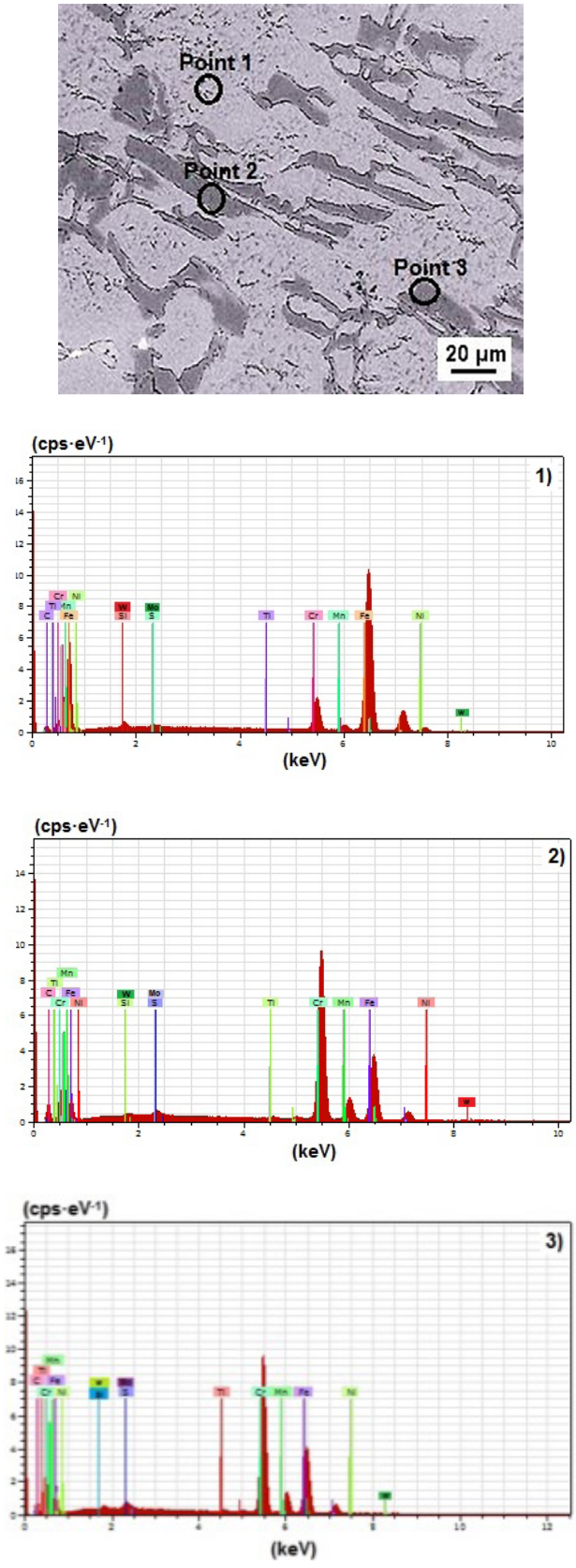

Figure 5. Chemical composition clarified by EDS of sample S5.

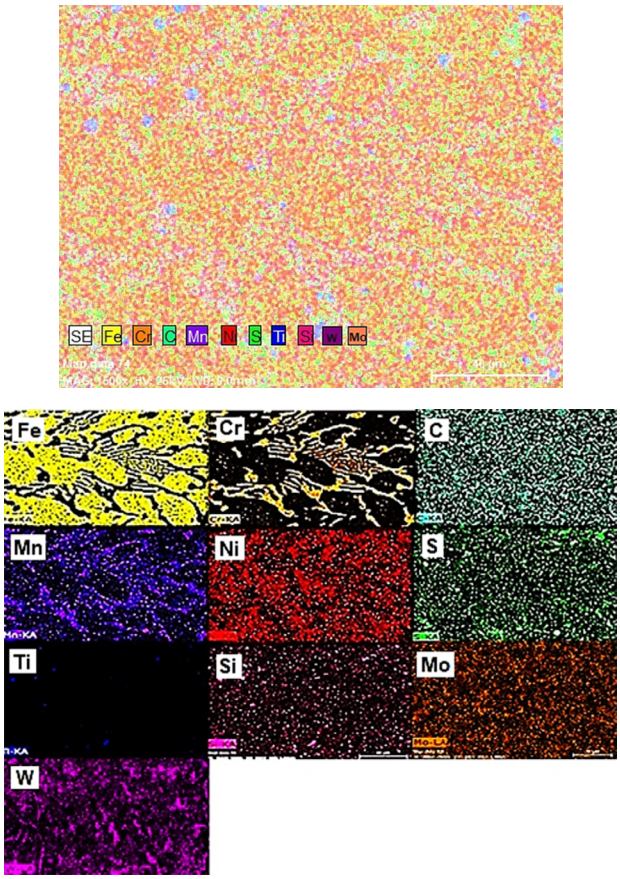

Figure 6. SEM mapped image analysis of sample S5.

heat-treated conditions. The presence of more than 6 wt.% Ni in the structure stabilized the austenite.

The DTA plot is given in Fig. 7. DTA analysis values obtained from four samples are given in Table 3. The solidification limit was observed based on the liquid and solidification temperatures in samples having increased Ni concentration from 0.5 to 6 wt.% (Fig. 2 and 5). All eutectic carbides and phases were identified at room temperature. Under unstable conditions, the phase transition interval was shorter than under equilibrium conditions. The liquidus temperature of the steel with 7 wt.% Ni (S5) content was higher than other samples. The sample having higher Ni concentration showed higher formation temperature of M_7C_3 and austenite. Additionally, in this alloy, M_3C precipitated earlier than the corresponding eutectic transformation in low-grade Ni samples (Biner, 1985; Chandan *et al.,* 2022). The presence of primary M_7C_3 carbides in our hypoeutectic samples were not expected. However, during the eutectic solidification, the carbides will completely reject Si and Ni into the remaining liquid. The remaining liquid then becomes supersaturated with Si and Ni, rising the activity coefficient of carbon, and the carbon content of eutectic boundary increases as the carbon concentration of hypereu-

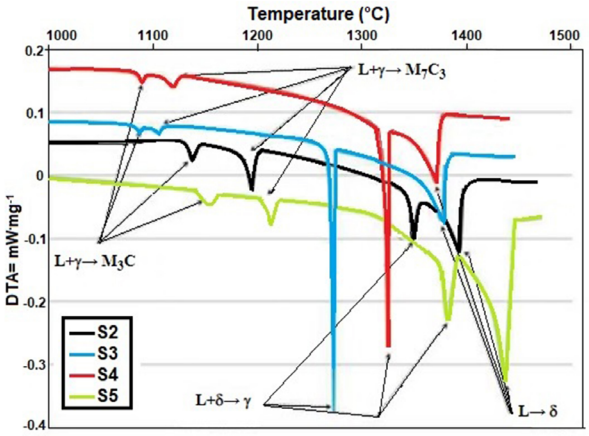

Figure 7. DTA plot of samples.

tectic liquid. Consequently, primary M_7C_3 carbides formed during solidification reactions (Table 3). If the Si level is not kept above 1.5%, the eutectic reaction (Rx3) drift down forming Rx4 which is not preferred.

3.2. Wear test

The change of friction coefficient as a function of load is shown in Fig. 8. The friction coefficient (μ) was determined to be more than 0.4 for various sample loads. An increase in the friction coefficient from the first value to the stable value was observed following ~1000 m sliding. For base samples, a major decrease in the friction was observed with load from ~1.0 for 40 N to ~ 0.62 for 140 N.

The worn surfaces for loads of 40, 90 and 140 N are shown in Fig. 9 a-c. A mild increase in the friction was observed at all loads with the increase in the austenite phase concentration. The austenite concentration nearly obtained the identical wear values in cast and heat-treated samples for 40 and 90 N loads. With the increase in the load to 140 N, certain differences were acquired in the as-cast and heat-treated conditions. At the above-mentioned

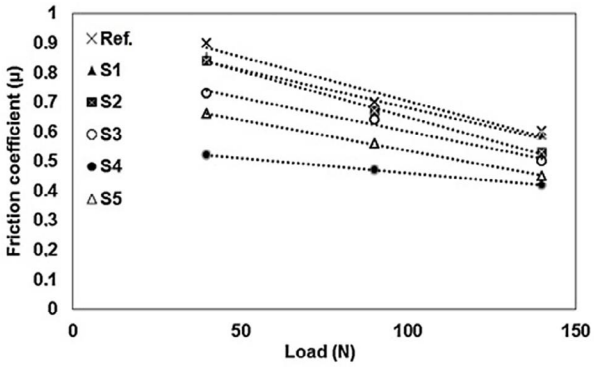

Figure 8. Change of friction coefficient as function of load.

Table 3. Values of DTA analyzes performed on four samples

Phases / Samples		S2 (°C)	S3 (°C)	S4 (°C)	S5 (°C)
Rx1	L→ d	1415	1420	1387	1425
Rx2	L+d→ g	1330	1367	1340	1380
Rx3	L+g→ M_7C_3	1185	1227	1120	1280
Rx4	L+g→ M_3C	1143	1145	1098	1158

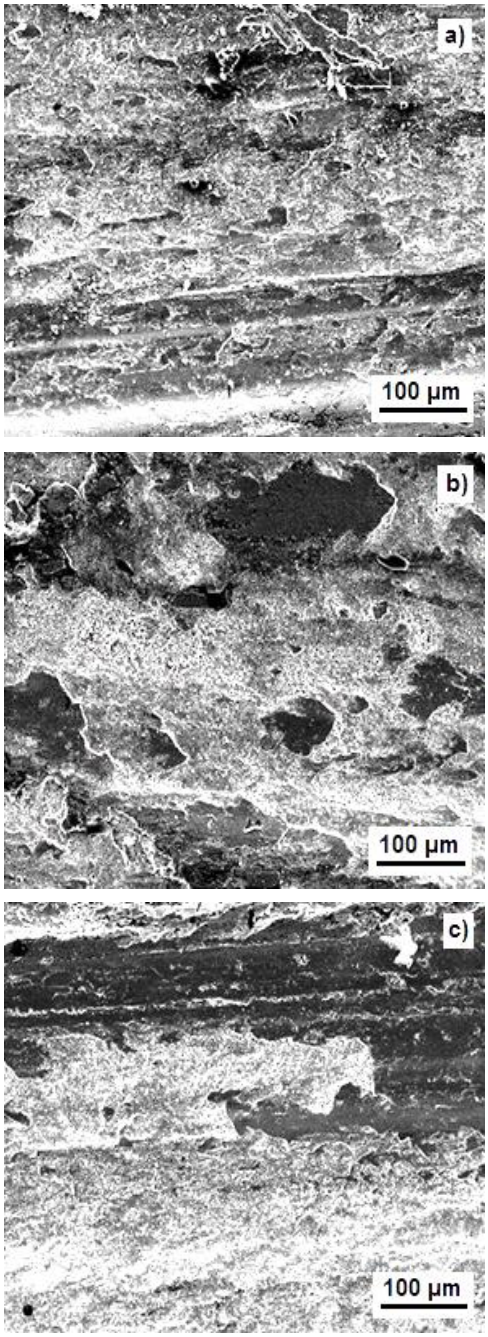

Figure 9. Worn surfaces at loads of a) 40 N, b) 90 N, c) 140 N.

loads, samples with 7 wt.% Ni (S5) exhibited the best wear resistance. Sample of as-cast form showed the weakest wear resistance. No differences in the composition surface structure were observed. In Fig. 9a, it could be observed that the worn surface of the reference sample without Ni content at 40 N was presented local grooves. The remaining regions were determined to have a uniform structure and smooth oxide layer. A carbide component was determined within the oxide film of the surface at the load of 40 N.

Wear rates versus sliding distance are given in Fig. 10 a-d. It was determined to be Fe_2O_3 in Fig. 10b. Phases α-Fe and carbide M_7C_3 were also present. Increasing the load to 90 N resulted in fewer abrasive grooves (Fig. 10b) and a smoother surface. Mostly Fe_2O_3, few traces of carbide M_7C_3 and wear residues occurred. However, α-Fe was not detected at 40 N load. Oxide layers and fine particulate oxide deposits formed the surface morphology. Almost no change in the structure of the eroded surface was observed at higher loads. However, surface roughening was detected, which is a sign of local adhesion. Together with Fe_2O_3, the Fe_3O_4 phase was present in the debris. Moreover, more intense plates seen on the wear surface caused an increase in the density of the oxide layer. The oxides were effortlessly solved at the load of 90 N. However, the surface did not change at 40 N load. At 140 N load, the oxide layer with M_7C_3 fragments was thicker (Fig. 10c). The expansion of carbide fragmentation was determined to be ~25 μm at the above-mentioned load. There were also incipient stages of carbide cracking by fragmentation of carbide rods adjacent to the surface. Nevertheless, a more diffuse interface was acquired. Numerous M_7C_3 particles obtained from an extremely deformed substrate layer were present in the oxide. The effect of M_7C_3 size and morphology as a result of Ni addition was clearly observed. The smallest carbide is equals to 7 wt.% Ni, and it caused a thinner and steadier deformation zone.

However, bigger sizes of cracks were observed in the surface deformation layer in the 6 wt.% Ni sample (S4) with bigger carbide particles. The development of the microstructure on the surface apart from the cracking grade was not affected in any way by the material composition. Deformation measurement were performed on the worn surface. Addition of up to 5 wt.% Ni resulted in reduced the carbide size, changed connectivity and an increase in volume fraction. An alteration in the solidification range resulted in the improvement of the structure because of Ni addition. The high Cr iron, hypoeutectic, but Ni changed the chemical content of the alloy adjacent to the single-phase structure and ultimately, a fully austenitic zone for sample with >6 wt.% Ni. There is a shorter solidification range in the single-phase structure, and the following tendency is

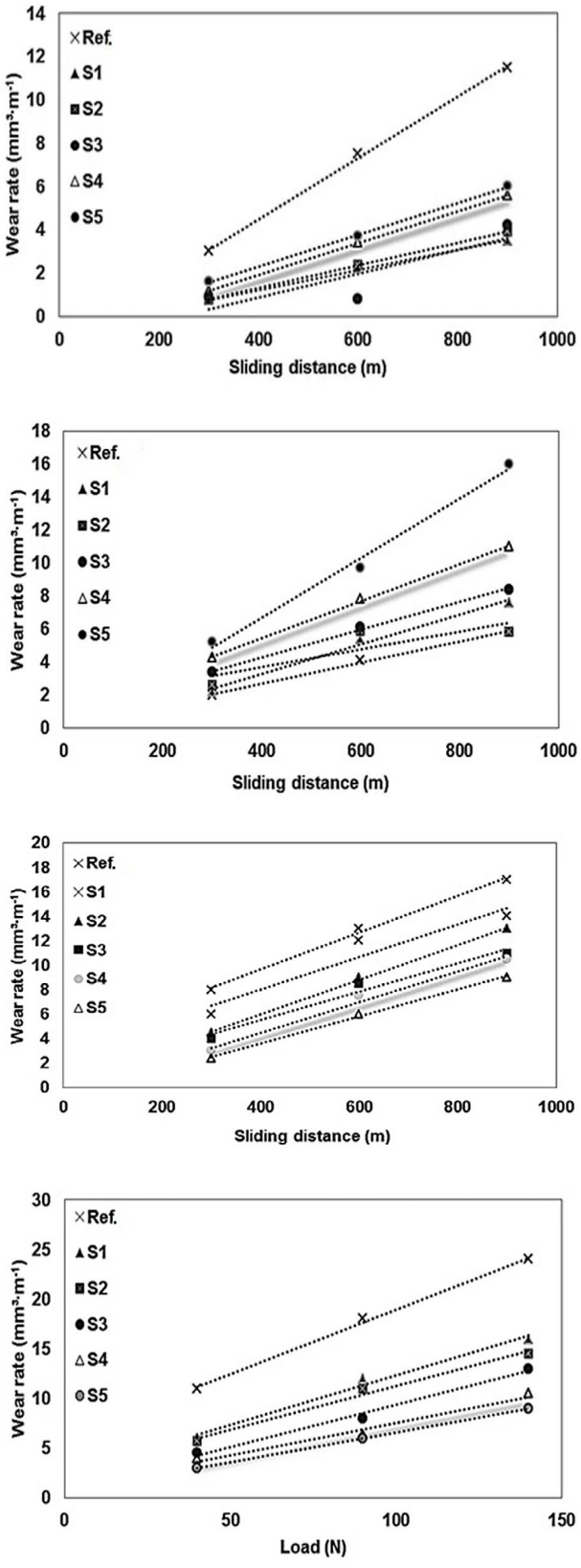

Figure 10. Wear rates versus sliding distance, a) 40 N load, b) 90 N load, c) 140 N load, d) Total wear rate at 900 m.

observed: a finer structure of the alloy is acquired in case of a shorter solidification range. Additionally, the austenite phase is stabilized by Ni, subject to the impact on solidification range, and an increase in the rate of Ni and a decline in the austenite content demonstrate this. This alteration was graded to 2 wt.% Ni (S2), yet heavy for 7 wt.% Ni (S5). A significant difference was observed in the microstructure of the 6 wt.% Ni (S4) addition and materials with eutectoid transformation properties created pearlitic structures. An alteration in the ratio of secondary carbides represents a complementary impact of adding Ni. The accessible the carbon consequent for deposition on tempering was increased by Ni, subject to carbide fraction (Lin *et al*., 2010; Chandan *et al.,* 2022). The mechanism of wear was predominantly oxidational at every load. However, at lower loads, there was an indication of abrasive grooving. Load generally increased the oxide layer thickness. At low loads, metallic abrasion was demonstrated by the wear debris composition, however, just oxidational wear was observed at the load of 140 N. There was an alteration in the composition of the oxide debris by the load. XRD patterns of worn particulates obtained from the surface of sample S5 during wear tests are displayed in Fig. 11. At low loads, it was totally Fe_2O_3, and at high loads, it was the Fe_2O_3 and Fe_3O_4 combination.

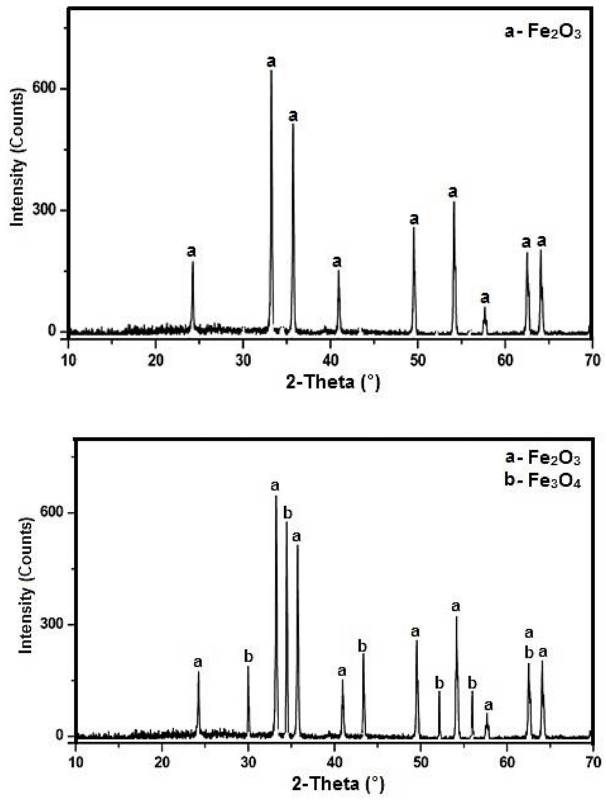

Figure 11. XRD patterns of worn particulates obtained from surface of sample S5.

With an increase in the load, the M_7C_3 content in the oxide increased. A reduction in the secondary dendrite arm spacing constituted the single important microstructural impact (Biner, 1985; Laird *et al*., 2000). Nevertheless, there was no major change in the carbide volume fraction. No significant impact of Ni on wear behavior was observed particularly at 140 N. A load 90-140 N slightly reduced the wear coefficient for 1-2 wt.%.

4. CONCLUSIONS

- Ni had a substantial impact on reducing the arm distance of the secondary dendrite arm spacing.
- A little rise on the hardness was obtained for the heat-treated samples having Ni concentration up to 2 wt.%. Hardness decreased with more than 2 wt.% Ni.
- The wear coefficient of all samples under a load of 90 N decreased due to a denser surface oxide film and reduction in metal wear.
- An oxide layer consisting of Fe_2O_3 and Fe_3O_4 and M_7C_3 residues caused almost no change in the wear resistance of samples containing 2% Ni under 40-140 N loads.
- The increase of Ni as 2-4 wt.% resulted in an increase in the wear coefficient under loads of 40-140 N.
- The samples having Ni concentration over 4 wt.% showed higher formation temperature of M_7C_3 and austenite.

ACKNOWLEDGMENTS

The authors are grateful to the Inan Machina Industry and Trade Inc. for their assistance in conducting the experiments.

DISCLOSURE STATEMENT

No potential conflict of interest was reported by the authors.

REFERENCES

Aso, S., Goto, S., Komatsu, Y., Hartono, W. (2001). Sliding wear of graphite crystallized chromium white cast iron. *Wear.* 250 (1-12), 511–517. https://doi.org/10.1016/S0043-1648(01)00600-7.

Bedolla-Jacuide, A., Arias, L., Hernández, B. (2003). Kinetics of secondary carbides precipitation in a high-chromium white iron. *J. Mater. Eng. Perform*. 12, 371–382. https://doi.org/10.1361/105994903770342881.

Biner, S.B. (1985). The role of eutectic carbide morphology on the fracture behaviour of high-chromium cast irons–I. Austenitic alloys. *Canadian J. Metal. Mater. Sci.* 24 (2), 155–162. https://doi.org/10.1179/cmq.1985.24.2.155.

Chandan, A.K., Kishore, K., Hung, P.T., Ghosh, M., Chowdhury, S.G., Kawasaki, M., Gubicza, J. (2022). Effect of nickel addition on enhancing nano-structuring and suppressing TRIP effect in Fe40Mn40Co10Cr10 high-entropy alloy during high-pressure torsion. *Int. J. Plast.* 150, 103193. https://doi.org/10.1016/j.ijplas.2021.103193.

Chung, R.J., Tang, X., Li, D.Y., Hinckley, B., Dolman, K. (2009). Effects of titanium addition on microstructure and wear resistance of hypereutectic high chromium cast iron Fe-25wt.%Cr-4wt.%C. *Wear* 267 (1-4), 356–361. https://doi.org/10.1016/j.wear.2008.12.061.

Filipovic, M., Kamberovic, Z., Korac, M., Gavrilovski, M. (2013). Microstructure and mechanical properties of Fe–Cr–C–Nb white cast irons. *Mater. Des.* 47, 41–48. https://doi.org/10.1016/j.matdes.2012.12.034.

Hanlon, D.N., Rainforth, W.M., Sellars, C.M. (1999). The rolling/sliding wear response of conventionally processed and spray formed high chromium content cast iron at ambient and elevated temperature. *Wear* 225–229 (1), 587–599. https://doi.org/10.1016/S0043-1648(99)00053-8.

Kasama, A.H., Mourisco, A.J., Kiminami, C.S., Botta Fo, W.J., Bolfarini, C. (2004). Microstructure and wear resistance of spray formed high chromium white cast iron, *Mater. Sci. Eng. A.* 375-377, 589–594. https://doi.org/10.1016/j.msea.2003.10.093.

Laird, G., Gundlach, R., Röhrig, K. (2000). *Abrasion resistant cast iron handbook*. American Foundry Society, USA, pp. 1–222.

Lin, C.M., Chang, C.M., Chen, J.H., Wu, W. (2010). The effects of additive elements on the microstructure characteristics and mechanical properties of Cr–Fe–C hard-facing alloys. *J. Alloys Compds*. 498 (1), 30–36. https://doi.org/10.1016/j.jallcom.2010.03.127.

Lu, B., Luo, J., Chiovelli, S. (2006). Corrosion and wear resistance of chrome white irons—A correlation to their composition and microstructure. *Metall. Mater. Trans. A.* 37, 3029–3038. https://doi.org/10.1007/s11661-006-0184-x.

Mandal, S.S., Ghosh, K.S., Mondal, D.K. (2017). Correlation between microstructure, hardness, wear and electrochemical behaviour in 8.0%, 16.0% and 20.0% (by wt) chromium white irons. *Mater. Chem. Phys.* 193, 401–412. https://doi.org/10.1016/j.matchemphys.2017.02.041.

Mousavi Anijdan, S.H., Bahrami, A., Varahram, N., Davami, P. (2007). Effects of tungsten on erosion–corrosion behavior of high chromium white cast iron. *Mater. Sci. Eng. A*. 454-455, 623–628. https://doi.org/10.1016/j.msea.2006.11.128.

Pearce, J.T.H. (1983). The use of transmission electron microscopy to study the effects of abrasive wear on the matrix structure of a high chromium cast iron. *Wear* 89 (3), 333–344. https://doi.org/10.1016/0043-1648(83)90154-0.

Powell, G.L.F., Laird II, G. (1992). Structure, nucleation, growth and morphology of secondary carbides in high chromium and Cr-Ni white cast irons. *J. Mater. Sci.* 27, 29–35. https://doi.org/10.1007/BF00553833.

Powell, G.L.F., Bee, Y.J.V. (1996). Secondary carbide precipitation in an 18 wt.%Cr-1 wt.% Mo white iron. *J. Mater. Sci.* 31, 707–711. https://doi.org/10.1007/BF00367889.

Scandian, C., Boher, C., de Mello, J.D.B., Rézaï-Aria, F. (2009). Effect of molybdenum and chromium contents in sliding wear of high-chromium white cast ıron: The relationship between microstructure and wear. *Wear* 267 (1-4), 401–408. https://doi.org/10.1016/j.wear.2008.12.095.

Tabrett, C.P., Sare, I.R. (2000). Fracture toughness of high-chromium white irons: Influence of cast structure. *J. Mater. Sci*. 3, 2069–2077. https://doi.org/10.1023/A:1004755511214.

Tang, X.H., Chung, R., Li, D.Y., Hinckley, B., Dolman, K. (2009). Variations in microstructure of high chromium cast irons and resultant changes in resistance to wear, corrosion and corrosive wear. *Wear* 267 (1-4), 116–121. https://doi.org/10.1016/j.wear.2008.11.025.

Turenne, S., Lavallée, F., Masounave, J. (1989). Matrix microstructure effect on the abrasion wear resistance of high-chromium white cast iron. *J. Mater. Sci.* 24, 3021–3028. https://doi.org/10.1007/BF0238566.

Wang, J., Li, C., Liu, H., Yang, H., Shen, B., Gao, S., Huang, S. (2006). The precipitation and transformation of secondary carbides in a high chromium cast iron. *Mater. Charac.* 56 (1), 73–78. https://doi.org/10.1016/j.matchar.2005.10.002.

Wang, J., Xiong, J., Fan, H., Yang, H.S., Liu, H.H., Shen, B.L. (2009). Effects of high temperature and cryogenic treatment on the microstructure and abrasion resistance of a high chromium cast iron. *J. Mater. Proces. Technol.* 209 (7), 3236–3240. https://doi.org/10.1016/j.jmatprotec.2008.07.035.

Zhang, M.X., Kelly, P.M., Gates, J.D. (2001). The effect of heat treatment on the toughness, hardness and microstructure of low carbon white cast irons. *J. Mater. Sci.* 36, 3865–3875. https://doi.org/10.1023/A:1017949600733.

Zhi, X., Xing, J., Gao, Y., Fu, H., Peng, J., Xiao, B. (2008). Effect of heat treatment on microstructure and mechanical properties of a Ti-bearing hypereutectic high chromium white cast iron. *Mater. Sci. Eng. A*. 487 (1-2), 171–179. https://doi.org/10.1016/j.msea.2007.10.009.